Numerical verification of the continuous calculation method for tip stress during the driving process of the dynamic penetration test

Quoc Ahn Tran, Bastien Chevalier, Miguel Angel Benz-Navarrete, Pierre Breul, Roland Gourvès

Numerical verification of the continuous calculation method for tip stress during the driving process of the dynamic penetration test

Quoc Ahn Tran [a,b], Bastien Chevalier [a,*], Miguel Angel Benz-Navarrete [b], Pierre Breul [a], Roland Gourvès [b]

[a] *Université Clermont Auvergne, CNRS, SIGMA Clermont, Institut Pascal, F-63000 Clermont-Ferrand, France*
[b] *Sol-Solution, Géotechnique Réseaux, F-63200 Riom, France*

Abstract

This paper presents a calculation method for obtaining the continuous variation in stress between the tip and the soil during dynamic penetration tests, particularly in the case of using the Panda 3® penetration testing device. The originality of the method is that the tip stress can be computed continuously throughout the driving process. For each impact of the hammer on the penetrometer, data are recorded by sensors located at the top of the apparatus. Then, the stress at the tip and the displacement of the apparatus are calculated with a method based on the propagation of waves in the device. A three-dimensional numerical model of the penetration test, based on the Panda 3® specifications and using the discrete element method (DEM), is proposed in this paper. The purpose of the simulations is to validate the calculation method by comparing the curves of the tip stress versus the penetration distance obtained in two different ways, the first being the distance directly observed at the tip and the second being the distance calculated from the data recorded at the top of the penetrometer, as with the experimental device. The entire apparatus is represented, including the hammer, the rod, and the tip, and is driven into the model soil. The calculation method is applied, and the results are compared to the actual response of the soil to the driving of the penetrometer directly at the tip, which can be obtained with the numerical model. The responses are found to be very similar, confirming the theoretical framework and its underlying assumptions. This method is applied to dynamic penetration tests and provides the opportunity to obtain mechanical parameters other than the tip resistance from the tests.
© 2019 Production and hosting by Elsevier B.V. on behalf of The Japanese Geotechnical Society.

Keywords: Dynamic cone penetration test; Discrete element method; Tip resistance

1. Introduction

The penetration test is widely used for the characterization of soils in situ. The Panda penetrometer is a light dynamic penetrometer with variable input energy. It is used to drive a rod into the ground with a tip by means of a hammer. For each impact of the hammer, the energy supplied to the penetrometer and the response of the ground are measured (Gourvès, 1991). Conventionally, the tip resistance of the ground is obtained as a function of the depth (Fig. 1(a)).

With the latest technological evolutions of this device, called Panda 3®, it is possible to obtain, for each impact, a complete curve of the stress at the tip as a function of its penetration. This curve is obtained from the measurement and decoupling of the waves generated at impact and propagating in the apparatus (Benz-Navarrete, 2009).
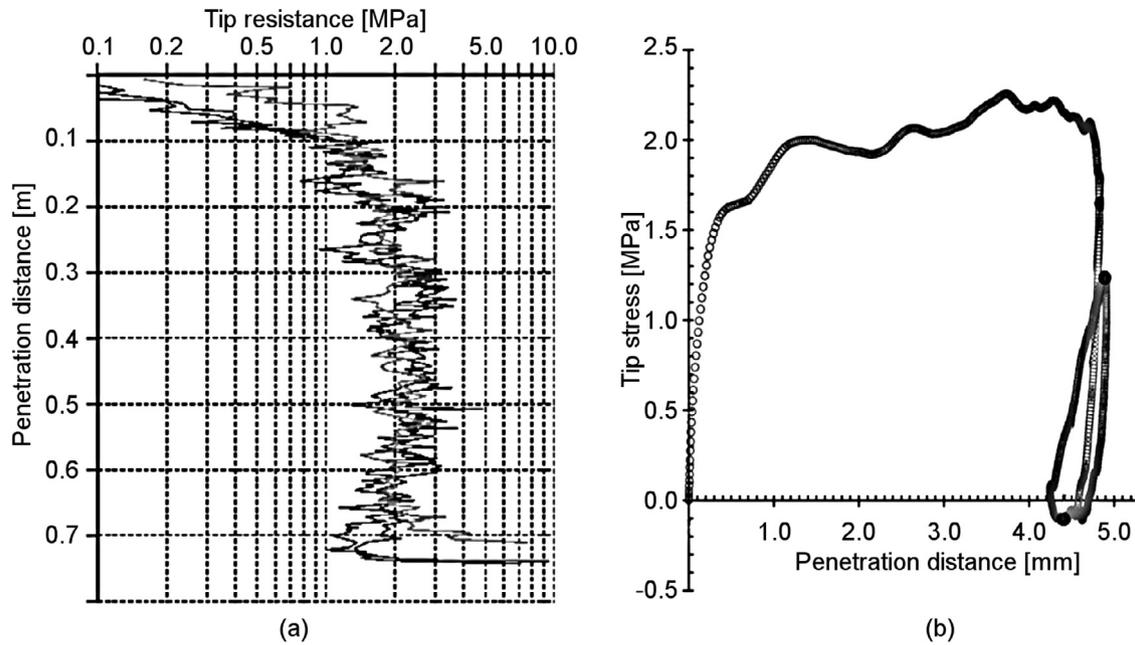

Fig. 1. Results obtained from dynamic penetration Panda 3® tests: (a) for complete tests in terms of tip resistance as a function of depth and (b) for a single impact on the penetrometer in terms of stress on the tip as a function of the tip penetration distance (Benz-Navarrete, 2009).

Fig. 1(b) shows an example of the results obtained for one impact.

Smith (1960) presented the formation and propagation of stress waves in one dimension based on Timoshenko (1934). This model is the basis of the wave equation modeling approach. When mass M, represented by the hammer, strikes the head of the penetrometer with speed v_{imp}, a compression wave, $u(x,t)$, is generated and travels at constant speed v_{rod} toward the tip. This compression wave follows the equation

$$\frac{\partial^2 u(x,t)}{\partial t^2} = \frac{1}{v_{rod}^2}\frac{\partial^2 u(x,t)}{\partial x^2} \qquad (1)$$

The general solution to Eq. (1) is represented by the superposition of two elementary waves, one traveling downward, u_{down}, and one traveling upward, u_{up}, as follows:

$$u(x,t) = u_{down}(\xi) + u_{up}(\zeta) \qquad (2)$$

with $\xi = t - \frac{x}{v_{rod}}$ and $\zeta = t + \frac{x}{v_{rod}}$.

During the propagation of each wave along the rod, wave $u(x, t)$ generates deformation $\varepsilon(x, t)$ at each position x, as described by Eq. (3). The particle velocity, $v(x, t)$, is also represented by the superposition of two elementary waves, namely,

$$\begin{cases} \varepsilon(x,t) = \varepsilon_{down}(\xi) + \varepsilon_{up}(\zeta) \\ v(x,t) = v_{down}(\xi) + v_{up}(\zeta) \end{cases} \qquad (3)$$

Wave propagation equations have been used in many applications in the field of geotechnical engineering. Rausche et al. (1985) developed the CASE method to back-calculate the soil resistance from the stress wave data collected during the installation of driven piles. The programs GRLWEAP and CAPWAP were developed to model the wave equation and to analyze the stress wave data, respectively, in order to back-calculate the soil resistance assuming the behavior models for the soil and the pile. Sy and Campanella (1991) used both programs to analyze the standard penetration test (SPT). Abou-Matar and Goble, 1997; Schmertmann, 1977 also used wave equations to study the SPT. These applications, however, require some assumptions for the behavior of the soil in order to back-calculate the soil resistance from the wave equations.

Several approaches exist in terms of measurement for the decoupling of the ascending and descending waves propagating in a solid. For example, the Hopkinson or Split Hopkinson Pressure Bar (SPHB) test method addresses the case of propagation in elastic or elastoplastic materials (Bacon, 1999; Zhao and Lok, 2002; Jacquelin and Hamelin, 2003, Bussac et al., 2002; Casem et al., 2003). In the SPHB test, it is possible to separate the waves traveling in one direction from those traveling in the other direction along the bar using only two strain sensors fixed at two different points on the bar (Bacon, 1999; Zhao and Lok, 2002). However, this method is susceptible to electromagnetic noise. In order to reduce the effect of the noise, it is possible either to use at least one additional sensor (Jacquelin and Hamelin, 2003; Bussac et al., 2002) or to replace one of the two strain sensors by an accelerometer, placed in the same section of the bar (Casem et al., 2003). In the case of the Panda 3 penetrometer, the method of wave decoupling is based on the work of Casem et al. (2003), in which both a strain sensor and an acceleration sensor are used. These sensors are fixed in the same position at the top of the apparatus.

From the measurements of force and velocity recorded by the sensors located near the anvil, deformation $\varepsilon(x, t)$ and particle velocity $v(x, t)$ can be recalculated for any point along the rod by separating the propagating waves in the rod. Thus, it is possible to reconstruct a priori the load-penetration curve at the tip of the penetrometer (Benz-Navarrete, 2009). Fig. 2 shows the force and velocity versus time, recorded during a single impact at a point located close to the top of the device, in samples of sand and ballast. Fig. 3 shows the results of the calculation of the stress versus penetration distance at the tip of the penetrometer for both materials.

The objective of this study is to reproduce the dynamic penetration test through numerical simulation by modeling a model soil and the whole apparatus to validate the method of calculation used in this type of measurement technique. The numerical model will record the same measurements as the actual device, i.e., at the top of the device. The wave decoupling method will be applied to these data to calculate the curve of the stress vs. penetration that takes place at the tip. The calculation results will be compared with the actual stress that is observed at the tip in the numerical model.

2. Numerical model

Numerous numerical studies using the two-dimensional discrete element method (DEM) have been employed to model the static penetration test (Huang and Ma, 1994; Huang and Hsu, 2004; Calvetti and Nova, 2005; Jiang et al., 2006a, 2006b; Jiang et al., 2014; Janda and Ooi, 2016) and the dynamic penetration test (Benz-Navarrete, 2009; Quezada et al., 2014; Escobar Valencia, 2015; Tran, 2015; Tran et al., 2016; Zhang et al., 2019). In these works,

the penetrometer was generally represented by a rigid solid that cannot deform. In the present study, a three-dimensional model is proposed to reproduce the dynamic penetration process employed in the Panda 3 test, including the behavior of the device (Tran et al., 2017a, 2017b) and using Itasca PFC^{3D} (Itasca, 2014). A realistic response, from the granular material in which the dynamic penetration tests are conducted, was needed, so DEM was chosen for this purpose. The modeling of the apparatus and the model soil are presented below.

2.1. Modeling the apparatus

Fig. 4(a) shows a view of the model of the penetrometer based on the Panda 3 specifications. The model hammer corresponds to the standard hammer used with the Panda 3 penetrometer. The model hammer is modeled by a single sphere with a diameter of 6 cm and a mass equal to 1.69 kg. The anvil is modeled by a sphere with a diameter of 3 cm and a mass equal to 0.75 kg. It is bonded to a steel rod, represented by a stack of spheres, with a diameter of 1.4 cm aligned vertically for a total length of 1.0 m. The tip, with a diameter of 2.25 cm, is modeled by wall elements reproducing the exact shape of the device; the cylindrical part has a diameter of 16 mm and a height of 20 mm, ending with a spike having an aperture angle of 90°. Fig. 4(b) shows the penetration testing device driven once into the sample of granular material.

The numerical model of the apparatus involves two types of contact models. In between the elements constituting the anvil, the steel rod, and the tip, a linear contact bond model is used to simulate the mechanical behavior of a continuous piece of steel. For all other contacts, the linear contact law is used. For both types of contacts, the
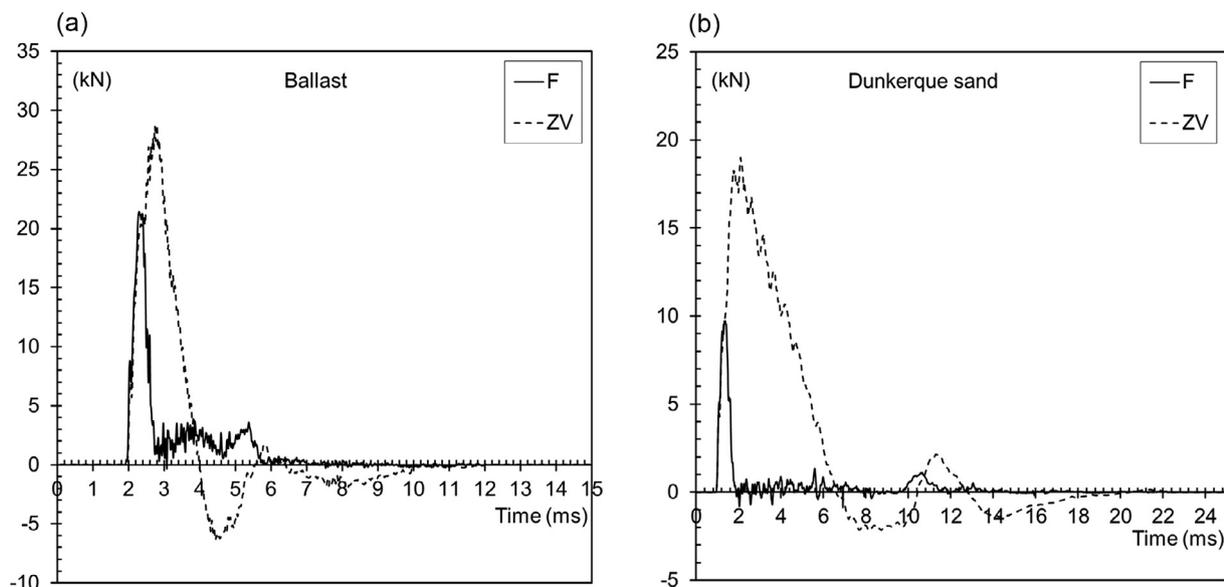

Fig. 2. Force and velocity multiplied by rod impedance measured at the top of the penetrometer, as a function of time, for an impact of the hammer on the penetration device: (a) tests in ballast and (b) tests in Dunkerque sand.
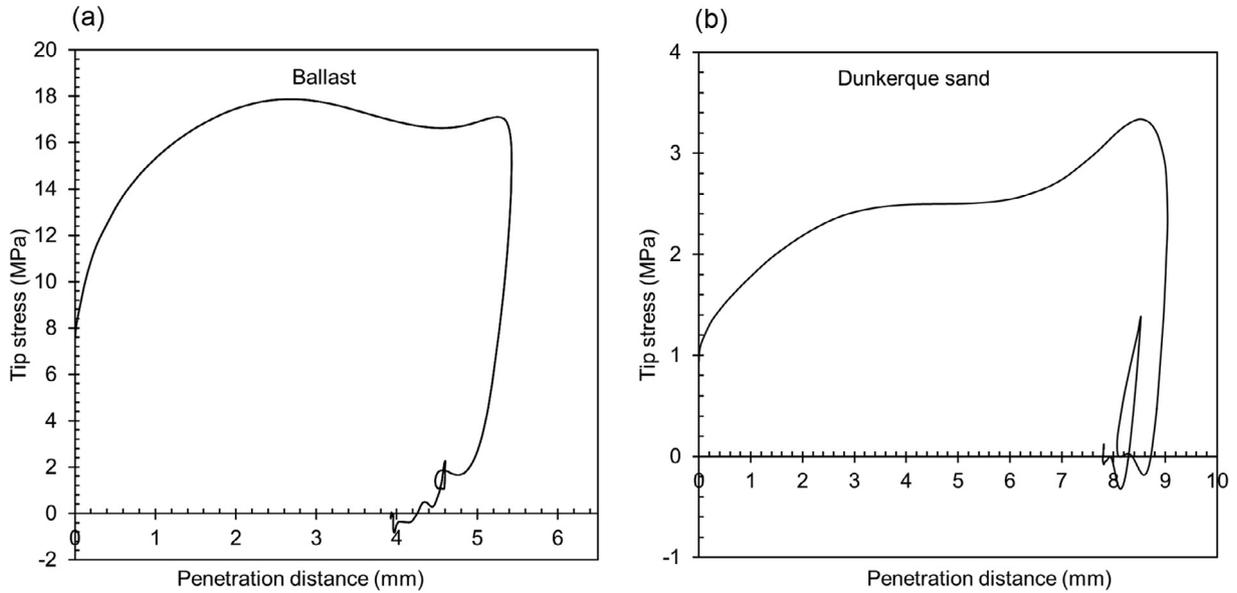
Fig. 3. Tip stress versus penetration distance calculated at the tip of the penetrometer, for an impact of the hammer on the penetration device: (a) tests in ballast and (b) tests in Dunkerque sand.
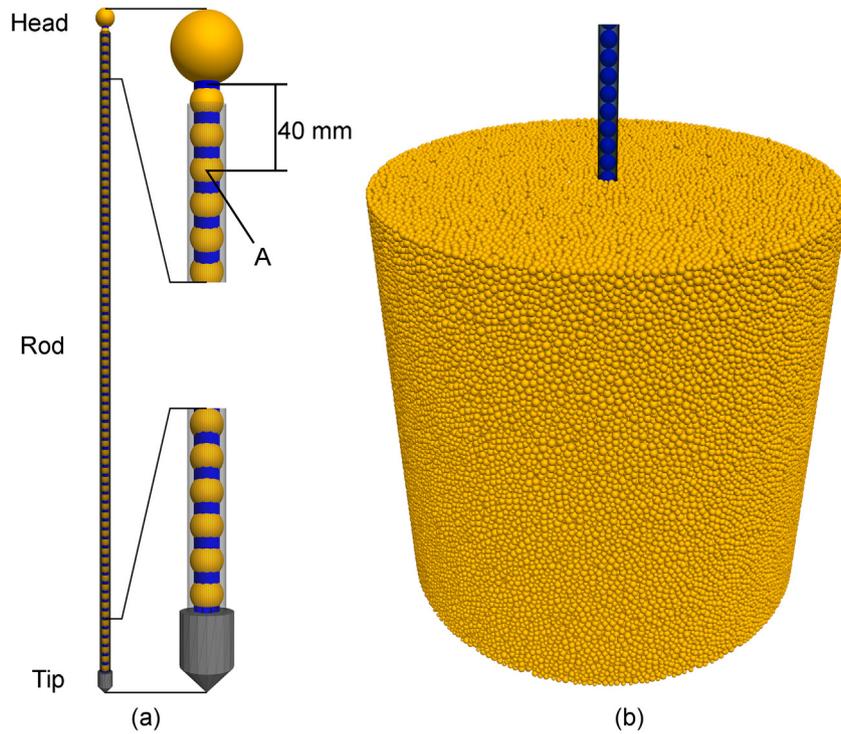
Fig. 4. Numerical model: (a) view of the model representing the penetration test device, based on the Panda 3 specifications, and (b) view of the penetrometer driven in a sample of spheres.

spring stiffness in the normal and shear directions, k_N and k_S, are calculated from contact modulus E^* and normal-to-shear stiffness ratio κ^*, as follows:

$$k_N = \frac{\pi \min(R_1, R_2)^2 E^*}{R_1 + R_2} \quad \text{and}$$

$$k_S = \frac{k_N}{\kappa^*} \quad \text{for sphere} - \text{sphere contact} \tag{4}$$

$$k_N = \frac{\pi R_1^2 E^*}{R_1} \quad \text{and}$$

$$k_S = \frac{k_N}{\kappa^*} \quad \text{for sphere} - \text{wall contact} \tag{5}$$

where R_1 and R_2 are the radii of the contacting spheres.

For contacts where a linear contact bond model was installed, a bond in the normal direction prevents the contact from breaking. The maximal limit in tension of the

bond was set to a very high value because the stress level reached in the simulations is much smaller than the actual limit tension of steel. In the shear direction, no bond was necessary because steel particles were blocked from displacement in the horizontal plane. For these contacts, normal stiffness k_N was calculated based on Eq. (4) with the Young modulus of steel of $E^* = 2.06 \times 10^5$ MPa. The tangential stiffness was calculated with a stiffness ratio of κ^* of 2.71, but it has no importance here since no relative displacement is allowed between the steel particles.

For the contact between the hammer and the anvil, the linear stiffness was calibrated by simulating impact tests; normal stiffness k_N was determined with Eq. (4) in order to obtain the same relation between the maximal impact force in the anvil and the impact velocity as in the experimental tests. The value of the contact modulus of $E^* = 3.05 \times 10^2$ MPa was obtained. Fig. 5 shows the variation between the maximal impact force in the anvil and the impact velocity obtained in the experimental tests and the numerical simulation. For the same reasons as in between the steel particles, the tangential stiffness was calculated with a stiffness ratio of κ^* of 2.71, but it plays no role here since no relative displacement is allowed between the hammer and the anvil during impact.

3. Modeling the soil

The penetrometer is driven into the model soil represented by a coarse granular material. The soil sample consists of spherical particles arranged in a cylindrical mold
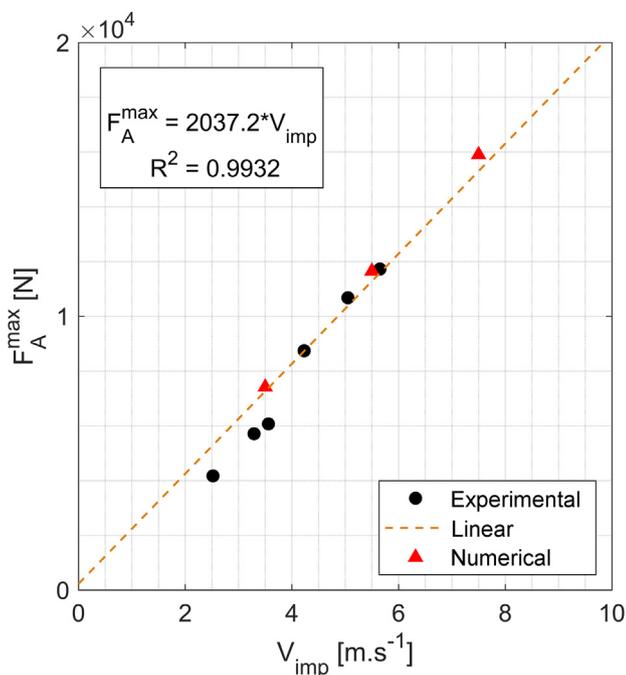

Fig. 5. Comparison of the maximum impact force obtained in the experimental impact tests with the response of the numerical model, with the value of the contact modulus of $E^* = 3.05 \times 10^2$ MPa between the hammer and the anvil.

with a diameter of 40 cm and a height of 40 cm. The cylindrical mold is made of one rigid wall and its diameter is constant throughout the simulation. The grain sizes are uniformly distributed between the diameters of 3.5 and 7.0 mm. The particles are generated smaller in size than their final size; they increase gradually until a dense packing is reached, corresponding to a void ratio of 0.54. A linear contact model was used for all contacts involving soil particles, i.e., in between the soil particles, between the soil particles and the penetrometer (tip and rod), and between the soil particles and the walls of the soil box. A contact modulus of $E^* = 2.00 \times 10^2$ MPa was used to calculate the normal spring stiffness in the contacts between the soil particles and between the soil particles and the penetrometer. A contact modulus of $E^* = 2.00$ MPa was used to calculate the spring stiffness between the soil particles and the walls. These values for the contact modulus ensure that the overlapping particles during the simulation remain small enough compared to their diameter. Apart from this reason, the effect of the normal spring stiffness is not of major importance in the process of dynamic penetration because of the large deformations that are involved. The values for the tangential spring stiffness were calculated with Eq. (5) and a stiffness ratio of κ^* of 3.33. A Coulomb friction criterion was considered with a coefficient of $\mu = 0.7$ in the contacts between the soil particles and with a coefficient of $\mu = 0.3$ between the soil particles and the tip of the penetrometer. For the contacts between the soil particles and the other walls, a coefficient of $\mu = 0$ was considered. A viscous damping ratio was considered in the normal direction for the contacts existing in-between the soil particles. The damping constant was taken as being equal to 10% of the critical damping constant, corresponding to a coefficient of restitution of 0.72.

Then, gravity is applied as well as a constant vertical confining stress equal to 40 kPa. The vertical confining pressure is a way to model the test as if it were conducted deeper in the soil layer, but without having to increase the number of particles. After the sample of soil particles is generated, the penetrometer is finally generated and driven down, first at a constant speed of 1.0 m s^{-1} until a depth of 15 cm is reached. The penetration speed used here is intentionally large in order to reduce the calculation time of this phase. The rod of the penetrometer is represented by a vertical stack of spheres. However, to avoid any contact or friction between the soil particles and the spheres representing the rod, the rod of the penetrometer is driven into the soil surrounded by a cylindrical wall whose diameter is slightly greater than the diameter of the spheres of the rod. No friction between this cylindrical wall and the soil particles can occur; the friction coefficient is set to $\mu = 0$ in the contacts between it and the soil particles.

After the stabilization of the whole system, dynamic penetration tests are conducted by impacting the hammer on the top of the penetrometer. The dynamic penetration tests are performed by the impact of a sphere representing the hammer on the top of the penetrometer, with velocities

of 1.75, 3.5 and 7.0 m s^{-1}, respectively, at the time of impact. A view of the soil sample with the penetrometer is shown in Fig. 4(b).

The values in Table 1 present the parameters for the different interactions used in the model.

4. Results

4.1. Application of wave decoupling

The method of separating the ascending and descending waves was applied to the results of the numerical model. Force F_A and velocity V_A of point A were recorded as functions of time. Point A corresponds to the location of the measurement device in the actual penetrometer in the upper part of the device; its location in the numerical model is shown in Fig. 4(a). The method of decoupling the waves traveling in the rod is applied in order to reconstruct the load-penetration curve at the tip. The assumptions underlying this method are explained in Benz-Navarrete (2009) and are given as follows:

- wave propagation in the rod is unidirectional, because the rod diameter is much smaller than the wavelengths;
- the impact of the hammer generates a single compression wave in the rod; there is no rebound of the hammer after the first impact;
- the rod is considered elastic, homogeneous, and uniform in its cross-section; Young's modulus E and density ρ are constant, and propagation velocity $v_{rod} = \sqrt{\frac{E}{\rho}}$ is also constant;
- the effects of the dispersion and damping of the waves along the rod are negligible;
- the external forces along the rod, especially the lateral friction, are ignored.

As compression waves are generated in the rod, force $F(x, \omega)$, velocity $v(x, \omega)$, and displacement $u(x, \omega)$ at any point along the rod can be expressed in the frequency domain, instead of the time domain, by operating a Fourier transformation. As a result of the above assumptions, expressions $F(x, \omega)$, $v(x, \omega)$, and $u(x, \omega)$ are given by the following equations:

$$F(x, \omega) = P(\omega) * e^{-i\frac{\omega}{v_{rod}}x} + N(\omega) * e^{+i\frac{\omega}{v_{rod}}x} \qquad (6)$$

$$v(x, \omega) = \frac{1}{Z}\left(P(\omega) * e^{-i\frac{\omega}{v_{rod}}x} - N(\omega) * e^{+i\frac{\omega}{v_{rod}}x}\right) \qquad (7)$$

$$u(x, \omega) = \frac{i\omega}{Z}\left(P(\omega) * e^{-i\frac{\omega}{v_{rod}}x} - N(\omega) * e^{+i\frac{\omega}{v_{rod}}x}\right) \qquad (8)$$

where

- x is the distance between measurement point A and the considered section;
- $P(\omega)$ is the wave traveling down and passing point A; $N(\omega)$ is the wave traveling up and passing point A;
- $Z = \rho v_{rod} A_{rod}$ is the impedance of the rod, with A_{rod} as the cross-section area of the rod and ρ as its density.

From the two quantities, $F_A(\omega)$ and $v_A(\omega)$, the two elementary waves at point A are determined by

$$P(\omega) = \frac{1}{2}(F_A(\omega) + Zv_A(\omega)) \qquad (9)$$

$$N(\omega) = \frac{1}{2}(F_A(\omega) - Zv_A(\omega)) \qquad (10)$$

Fig. 6 shows an example of the measurement recorded in the simulations at point A and the results of the calculation of the elementary compression waves (Eqs. (9) and (10)).

Once the forces corresponding to the ascending and descending waves have been determined at point A, it is possible to deduce the force acting at the bottom end of the rod, i.e., at the tip, by a procedure for the phase shift in the frequency domain (Eq. (6)). Finally, an inverse Fourier transform is necessary to obtain the tip force in the time domain. Eqs. (7) and (8) are used to determine the velocity, and thus, the penetration distance of the tip.

The calculated stress at the tip can be compared to the actual stress at the tip of the penetrometer. The values of the stress at the tip, both calculated and observed, are compared in Fig. 7 for the three impact velocities of 1.75, 3.5, and 7.0 m s^{-1}. They are represented as a function of the tip penetration distance. The reconstructed curve conforms to that obtained directly at the tip. The comparison of the calculated stress and the stress actually observed at the tip is seen to be very good. The slight gap between the two curves can be explained by the change in impedance existing at the transition between the rod and the tip, where the diameter changes from 1.4 cm to 2.25 cm.

Table 1
Parameters of the contact interactions between the different elements of the mechanical system.

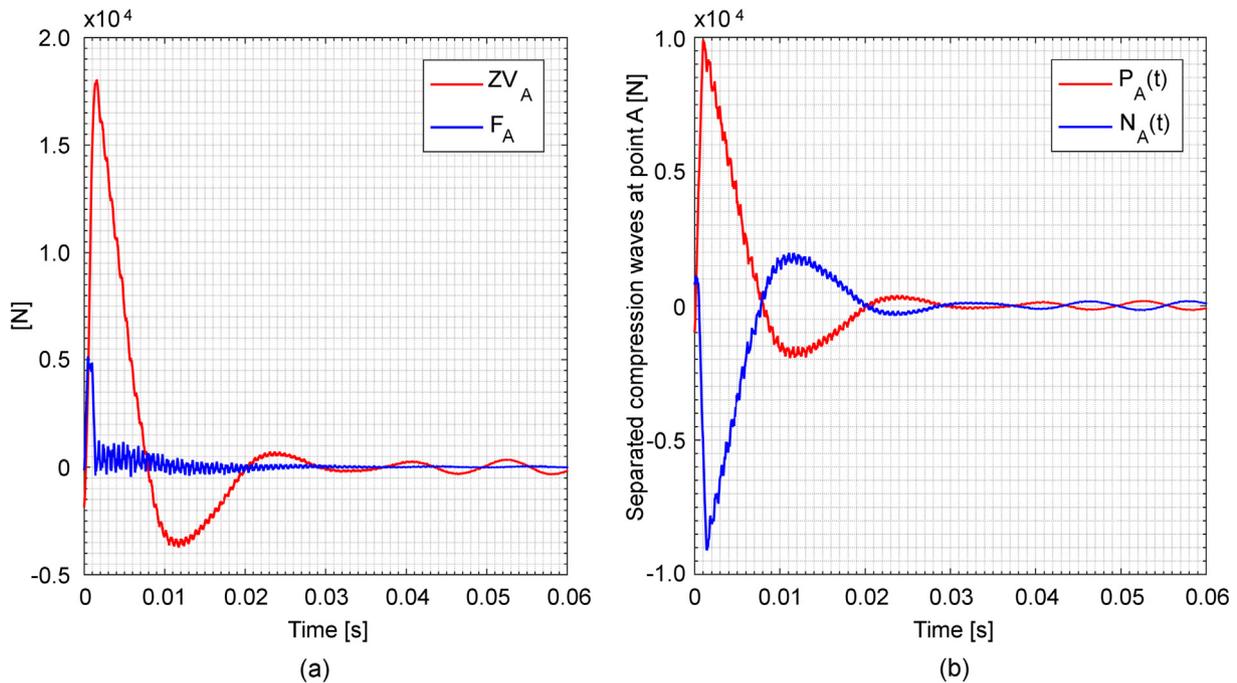| Interaction	Contact model	E* [MPa]	κ*	μ
Hammer vs. anvil	Linear model	3.05×10^2	2.71	0.0
Anvil vs. rod	Linear contact bond model	2.06×10^5	2.71	0.0
Rod vs. tip	Linear contact bond model	2.06×10^5	2.71	0.0
Tip vs. soil	Linear model	2.0×10^2	3.33	0.3
Soil vs. rod	Linear model	2.0×10^2	3.33	0.0
Soil vs. container boundaries	Linear model	2.0	3.33	0.0
Soil vs. soil	Linear model	2.0×10^2	3.33	0.7

Fig. 6. (a) Measurements at point A, force F_A, and velocity V_A, as functions of time after the impact, and (b) Results of the calculation of elementary compression waves passing point A, as functions of time, after the impact: P_A is the descending wave and N_A is the ascending wave.
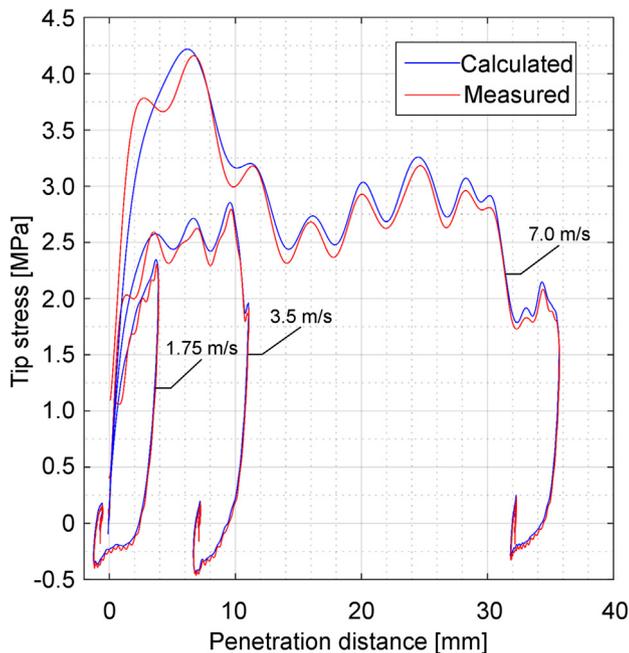

Fig. 7. Comparison of the stress between the tip and the soil for impact velocities of 1.75, 3.5, and 7.0 m s^{-1}, obtained by the wave separation method (blue line) and actually observed at the tip of penetrometer (red line).

5. Conclusion

With the ease and affordability of miniaturized and more accurate electronic components, measurement techniques in the geotechnical field have evolved a lot recently.

An example of the dynamic penetration test was presented and modeled in this paper, illustrated by the case of the Panda 3 penetrometer. It is possible to record and calculate the response of the soil at the tip of the penetrometer, caused by the impacts, continuously throughout the driving process.

In this paper, the process of the test was reproduced numerically to verify whether the behavior of the soil, i.e., at the tip, could be effectively and accurately calculated from the data recorded at the top of the device. A discrete model was used because of its ability to reproduce the system, composed of both the apparatus and a model soil, which was represented here by a coarse granular material.

The calculation method was based on the decoupling of the ascending and descending compression waves that travel along the rod of the penetrometer. The application of this method to the results obtained with the numerical model provided the supposed mechanical response of the soil at the tip, in the form of the stress at the tip as a function of its penetration distance. The results showed a good correspondence between the calculated curve and the one observed at the tip; the order of magnitude of the stresses was the same, the major oscillations of the curve were observed at the same moment, and the part representing the unloading was also very accurate.

The results obtained in this study are very promising for the experimental measurement technique because they conformed to the theory and confirmed that the assumptions associated with the theoretical framework are verified. Based on this curve, the potential of the dynamic penetration test has increased in the sense that other mechanical

properties could be extracted from this new source of information.

References

Abou-Matar, H., Goble, G., 1997. SPT dynamic analysis and measurements. ASCE J. Geotech. Geoenviron. Eng. 123 (10), 921–949.

Bacon, C., 1999. Separation of waves propagating in an elastic or viscoelastic Hopkinson pressure bar with three-dimensional effects. Int. J. Impact Eng. 22 (1), 55–69.

Benz-Navarrete, M.A., 2009. Mesures dynamiques lors du battage du pénétromètre Panda 2. Université Blaise Pascal-Clermont-Ferrand II, Clermont-Ferrand.

Bussac, M., Collet, P., Gary, G., Othman, R., 2002. An optimization method for separating and rebuilding one-dimensional dispersive waves from multi-point measurements. Application to elastic or viscoelastic bars. J. Mech. Phys. Solids 50 (2), 321–349.

Calvetti, F., Nova, R., 2005. Micro–macro relationships from DEM simulated element and in-situ tests. In: Proceedings of the International Conference on Powders & Grains 2005. CRC Press, Stuttgart, pp. 245–250.

Casem, D., Fourney, W., Chang, P., 2003. Wave separation in viscoelastic pressure bars using single-point measurements of strain and velocity. Polym. Test. 22 (2), 155–164.

Escobar Valencia, E.J., 2015. Mise au point et exploitation d'une nouvelle technique pour la reconnaissance des sols: le Panda 3. Université Blaise Pascal-Clermont-Ferrand II, Clermont-Ferrand.

Gourvès, R., 1991. Pénétromètre dynamique léger à énergie variable. Clermont-Ferrand, Université Blaise Pascal, France, 1991.

Huang, A., Ma, M., 1994. An analytical study of cone penetration tests in granular material. Can. Geotech. J. 31 (1), 91–103.

Huang, A., Hsu, H., 2004. Advanced calibration chambers for cone penetration testing in cohesionless soils. In: Geotechnical and Geophysical Site Characterization: Proceedings of the Second International Conference on Site Characterization ISC-2, Rotterdam: Millpress, pp. 147–166.

Itasca Consulting Group, Inc., 2014. PFC-Particle Flow Code version 5.0. Itasca, Minneapolis.

Jacquelin, E., Hamelin, P., 2003. Force recovered from three recorded strains. Int. J. Solids Struct. 40 (1), 73–88.

Janda, A., Ooi, J., 2016. DEM modeling of cone penetration and unconfined compression in cohesive solids. Powder Technol. 293, 60–68.

Jiang, M., Yu, H., Harris, D., 2006a. Discrete element modeling of deep penetration in granular soils. Int. J. Numer. Anal. Meth. Geomech. 30 (4), 335–361.

Jiang, M., Harris, D., Zhu, H., 2006b. Future continuum models for granular materials in penetration analyses. Granular Matter 9 (1–2), 97–108.

Jiang, M., Dai, Y., Cui, L., Shen, Z., Wang, X., 2014. Investigating mechanism of inclined CPT in granular ground using DEM. Granular Matter 16 (5), 785–796.

Quezada, J., Breul, P., Saussine, G., Radjai, F., 2014. Penetration test in coarse granular material using contact dynamics method. Comput. Geotech. 55, 248–253.

Rausche, F., Goble, G.G., Likins, G.E., 1985. Dynamic determination of pile capacity. J. Geotech. Eng. 111 (3).

Schmertmann, J.H., 1977. Use the SPT to measure dynamic soil properties? -Yes, But..! Dynamic geotechnical testing, ASTM STP 654, American Society for Testing and Materials, pp. 341–355.

Smith, E.A.L., 1960. Pile driving analysis by the wave equation. ASCE J. Soil Mech. Foundations Div. 86 (SM4), 1960.

Sy, A., Campanella, R.G., 1991. Wave equation modeling of the SPT. In: Proc. ASCE Geotechnical Engineering Congress, Boulder, Colorado, June 9–12, 1991.

Timoshenko, S., 1934. Theory of elasticity. McGraw-Hill, Auckland.

Tran, Q.A., 2015. Modélisation numérique du comportement des milieux granulaires à partir de signaux pénétrométriques: approche micro-mécanique par la méthode des éléments discrets. Université Blaise Pascal-Clermont-Ferrand II, Clermont-Ferrand.

Tran, Q.A., Chevalier, B., Breul, P., 2016. Discrete modeling of penetration tests in constant velocity and impact conditions. Comput. Geotech. 71, 12–18.

Tran, Q.A, Chevalier, B., Breul, P., 2017. Effect of the characteristics of granular media on dynamic penetration test - Numerical study using 2D – DEM. In: EPJ Web Conf. (140): Powders & Grains 2017. doi: 10.1051/epjconf/201714016004.

Tran, Q.A, Chevalier, B., Benz-Navarrete, Breul, P., Gourvès, R., 2017. Modeling of light dynamic cone penetration test Panda 3R in granular material by using 3D Discrete element method. In: EPJ Web Conf. (140): Powders & Grains 2017. doi: 10.1051/epjconf/201714016003.

Zhao, P., Lok, T., 2002. A new method for separating longitudinal waves in a large diameter Hopkinson bar. J. Sound Vib. 257 (1), 119–130.

Zhang, N., Arroyo, M., Ciantia, M.O., Gens, A., Butlanska, J., 2019. Standard Penetration Testing 1 in a virtual calibration chamber. Comput. Geotech. 111, 277–289.